nanomaterials

Article

Potassium-Based Solid Sorbents for CO_2 Adsorption: Key Role of Interconnected Pores

Yuan Zhao [1], Jiangbo Huo [2,*], Xuefei Wang [1] and Shunwei Ma [1]

[1] Tianjin College, University of Science and Technology Beijing, Tianjin 301830, China; zhaoyuan01277@sina.com (Y.Z.)
[2] Tianjin Key Laboratory of Aquatic Science and Technology, School of Environmental and Municipal Engineering, Tianjin Chengjian University, Tianjin 300384, China
* Correspondence: huozhaoyuan@163.com; Tel.: +86-22-23085117

Abstract: Industrial CO_2 emissions contribute to pollution and greenhouse effects, highlighting the importance of carbon capture. Potassium carbonate (K_2CO_3) is an effective CO_2 absorbent, yet its liquid-phase absorption faces issues like diffusion resistance and corrosion risks. In this work, the solid adsorbents were developed with K_2CO_3 immobilized on the selected porous supports. Al_2O_3 had an optimum CO_2 adsorption capacity of 0.82 mmol g^{-1}. After further optimization of its pore structure, the self-prepared support Al_2O_3-2, which has an average pore diameter of 11.89 nm and a pore volume of 0.59 cm^3 g^{-1}, achieved a maximum CO_2 adsorption capacity of 1.12 mmol g^{-1} following K_2CO_3 impregnation. Additionally, the relationship between support structure and CO_2 adsorption efficiency was also analyzed. The connectivity of the pores and the large pore diameter of the support may play a key role in enhancing CO_2 adsorption performance. During 10 cycles of testing, the K_2CO_3-based adsorbents demonstrated consistent high CO_2 adsorption capacity with negligible degradation.

Keywords: CO_2; potassium carbonate; adsorbent; aluminum oxide

Citation: Zhao, Y.; Huo, J.; Wang, X.; Ma, S. Potassium-Based Solid Sorbents for CO_2 Adsorption: Key Role of Interconnected Pores. *Nanomaterials* **2024**, *14*, 1838. https://doi.org/10.3390/nano14221838

Academic Editor: Justo Lobato

Received: 30 September 2024
Revised: 8 November 2024
Accepted: 14 November 2024
Published: 17 November 2024

1. Introduction

The increasing concentration of CO_2 in flue gas from coal-fired power plants, a critical driver of the greenhouse effect, has led to the recognition that Carbon Capture and Storage (CCS) technology, particularly post-combustion capture, is regarded as a promising solution for the reduction of carbon dioxide emissions [1–6]. Although the liquid amine absorption method has been widely utilized in post-combustion capture, it still faces several challenges, including corrosiveness to containment vessels, potential amine volatility leading to environmental contamination, and significant mass transfer resistance within the liquid phase [7–10]. Recently, the incorporation of organic amines into porous supports has been extensively studied by many researchers [11–24]. Solid amine adsorbents, utilizing materials with high porosity such as polymers [11–13], carbon materials (e.g., carbon nanotube [14,15], activated carbon [16,17], and mesoporous carbon [18]), and mesoporous molecular sieves (e.g., SBA-15 [19–21], MCM-41 [22,23], and KIT-6 [24]), have been a focal point of research. These adsorbents incorporate various amine groups (e.g., primary, secondary, and tertiary amines) to enhance CO_2 capture capabilities [25]. However, despite their high adsorption capacity, the surface utilization rate of amine groups is still quite low. This is mainly because the organic amine has high viscosity and large molecular diameter, making it hard to penetrate evenly in the pores, which can lead to aggregation, pore blockage, and ultimately fewer active sites on the surface. Furthermore, there is significant amine loss during the adsorption–desorption cycles due to the facts that amines are inherently volatile organic compounds. Thus, it is necessary to develop innovative technologies or materials to overcome the current limitations in efficiency and cost.

In recent years, numerous studies have reported the use of potassium carbonate as an active component impregnated onto support materials to fabricate K_2CO_3-based adsorbents, which serve as a substitute for amine-based adsorbents for CO_2 capture [26–28]. Alkali carbonate-based adsorbents exhibit superior stability and are free from issues of secondary environmental pollution. They are more difficult to decompose, even when the temperature is increased to 800 °C. Generally, a temperature of 350 °C is adequate to fully regenerate the adsorbent. The inherent alkalinity of potassium carbonate confers a significantly enhanced CO_2 adsorption capacity upon the adsorbent, particularly effective for the capture of low-concentration CO_2, such as the 10–15% found in flue gasses. Current research on K_2CO_3-based adsorbents predominantly focuses on the in-depth exploration of the underlying reaction mechanisms and the selection of appropriate support materials [29–43]. The carbonation reaction induced by K_2CO_3-based sorbents was found to consist of two steps: first, the hydration reaction takes place, and then the produced $KHCO_3$ reacts rapidly. During the CO_2 sorption process, the carbonation reaction coexists with the adsorption process, indicating that both chemical and physical adsorption occur [28]. The support material in K_2CO_3-based sorbents facilitates not only physical CO_2 adsorption but also the dispersion of alkaline active sites. Consequently, the choice of support material and the optimization of its pore structure are crucial for enhancing the CO_2 adsorption performance of the sorbents.

Activated carbon was first considered as a superior support material due to its high surface area, abundant porosity, and controllable pore structure. It was reported that the K_2CO_3/AC sorbent exhibits high CO_2 capture capacities and rapid carbonation reaction rates [28–30]. Zeolites have also been widely investigated because they possess well-defined pore structures that can accommodate both the immobilized alkali metal carbonates and the adsorbed CO_2 [31–38]. In addition, activated alumina, with its high porosity, large surface area, and diverse pore channels, also has great potential for use as a support material [39–43]. Zhao et al. [40–43] have conducted extensive research on the supports for K_2CO_3-based sorbents. They impregnated potassium carbonate onto several supports and compared the conversion rates using thermogravimetric analysis (TGA) and a bubbling fluidized-bed reactor. However, the pore structure of the support materials requires additional refinement to optimize performance. There is an imperative to elucidate the correlation between the pore structural attributes and CO_2 adsorption efficacy, which is pivotal for informing the strategic design of advanced support materials. In this study, the performance of adsorbents prepared with various support materials was systematically compared, and the pore structure was further improved by strategically selecting the most suitable support. Additionally, the research endeavored to delineate the principal factors that influence CO_2 adsorption capacity.

2. Materials and Methods

2.1. Acquisition of the Support Materials

The porous solid materials, including ZSM-5, zeolite 5A, zeolite β, zeolite NaY, and MCM-41, served as supports and were obtained from Nanjing XFNANO Materials Tech Co., Ltd., Nanjing, China. The activated carbons, namely, CSAC and CAC, were purchased from Kecheng Activated Carbon Co., Ltd., Beijing, China. Aluminum oxide (Al_2O_3) was supplied by J&K Scientific. Moreover, two additional aluminum oxide supports were self-synthesized using the following procedures:

Scheme 1 [44]: In the preparation of Al_2O_3-1, 2.38 g of sodium aluminate, 20.23 g of urea, and 1 g of F127 were combined and dissolved in 70 mL of distilled water under vigorous stirring to form a homogeneous solution. This solution was subsequently transferred to a 100 mL Teflon-lined stainless steel autoclave, sealed, and subjected to hydrothermal treatment at 140 °C for 24 h. After that, the autoclave was cooled to ambient temperature, and then a white precipitate was formed. The resulting white precipitate was isolated from the supernatant and extensively washed with deionized water followed by ethanol in a sequential manner. The precipitate was then dried in a vacuum oven at 80 °C for 12 h.

Finally, the dried powder was calcined at 450 °C for 4 h in static air to yield the desired γ-Al_2O_3 product.

Scheme 2 [45]: For the synthesis of Al_2O_3-2, a mixture of $Al(NO_3)_3 \cdot 9H_2O$ (0.014 mol) and $CO(NH_2)_2$ (0.028 mol, 0.021 mol, or 0.056 mol) was dissolved in 70 mL of distilled water and stirred vigorously for 30 min to form a clear solution. The solution was then poured into a 100 mL Teflon-lined autoclave and heated at 180 °C (160 °C or 200 °C) for 4 h (3 h or 5 h), followed by natural cooling to room temperature. The resulting white precipitate was collected by vacuum filtration, washed sequentially with distilled water and anhydrous alcohol, and dried at 80 °C for 12 h in a vacuum oven. The boehmite precursor was calcined at 550 °C for 4 h, with a heating rate of 4 °C min^{-1}, to yield the final γ-Al_2O_3 product.

All the reagents used in the two schemes were of analytical grade without any further purification.

2.2. Preparation of K_2CO_3-Based Adsorbents

To prepare K_2CO_3-based sorbents, designated as x K_2CO_3/support, where x represents the weight percentage of K_2CO_3 in the adsorbents, a given amount of K_2CO_3 was first dissolved in 40 mL of methanol with stirring for 30 min at room temperature. Then, 2 g of the supports was added into the above K_2CO_3 methanol solution. After that, it was mixed with a magnetic stirrer at 40 °C until most of the methanol evaporated. Finally, the resultant x K_2CO_3/support adsorbents were further dried at 80 °C for 12 h under vacuum.

2.3. Characterization of the Self-Synthesized Al_2O_3

X-ray diffraction (XRD) spectra were obtained by an X'Pert PRO diffractor (PANalytical, Almelo, Holland, Cu Kα, λ = 0.15406 nm, 40 kV, 40 mA). The micro-morphology of the Al_2O_3 supports was observed by a scanning electron microscope (SEM, Hitachi SU8010, Tokyo, Japan). Before the measurements, the samples were degassed at 100 °C for 12 h under vacuum. Nitrogen adsorption–desorption isotherms were measured at 77 K using a Tristar II 3020 analyzer (Micromeritics, Norcross, GA, USA). The Brunauer–Emmett–Teller (BET) method was utilized to calculate the specific surface area. The total pore volume and pore size distribution were derived from the isotherm desorption branches using the Barrett–Joyner–Halenda (BJH) model. A thermogravimetric analysis (TGA, Netzsch STA 449F5, Selby, Germany) of samples was performed in a highly pure N_2 atmosphere at a flow rate of 70 mL/min. About 10 mg of the sample was heated at a constant rate of 10 °C/min from room temperature to 600 °C.

2.4. Evaluation for CO_2 Adsorption over K_2CO_3-Based Adsorbents

A fixed-bed flow sorption system, equipped with gas flow controllers and an integrated online gas chromatograph, was designed and constructed for the purpose of evaluating adsorbent performance in CO_2 adsorption, as depicted in Figure 1. The process involved packing 2 g of adsorbent into a U-shaped quartz reactor, which was placed in a programmable furnace for precise temperature control. Prior to each measurement, the sample was heated to 100 °C in a highly pure Ar stream at the flow rate of 100 mL min^{-1} for 60 min to eliminate the physically adsorbed H_2O and CO_2, and then the sample was cooled to 25 °C. The gas stream was rapidly switched to the 10% CO_2/air with 30% relative humidity (RH) at the desired flow rate of 10 mL min^{-1}. The moisture was produced by bubbling air into water, and the relative humidity was measured using a hygrometer. The flow rate of the gas was controlled by electronic flow control instruments. The concentrations of CO_2 at the inlet and outlet of the reactor were monitored by an online gas chromatograph (GC-7890II, Techcomp, Beijing, China) equipped with a methane converter, and the flame ionization detector was used. The sorption capacity of the adsorbent was calculated by the integration of the area above the breakthrough curve, and the integral equation is displayed in Equation (1)

$$q_s = \frac{1}{W} \times \left[\int_0^t Q \times \frac{C_0 - C}{1 - C} d_t \right] \times \frac{T_0}{T} \times \frac{1}{V_m} \quad (1)$$

where q_s is the saturated adsorption capacity of CO_2, mmol g^{-1}. W is the weight of the adsorbent, g. Q is the gas flow rate mL min^{-1}. C_0 and C are the influent and effluent CO_2 concentration, respectively, vol%. t denotes the adsorption time, min. T_0 is 273K. T is the gas temperature, 273K. V_m is 22.4 mL $mmol^{-1}$. q_s is defined as the adsorption capacity of CO_2 when C is equal to C_0; i.e., C/C_0 is equal to 1.0.

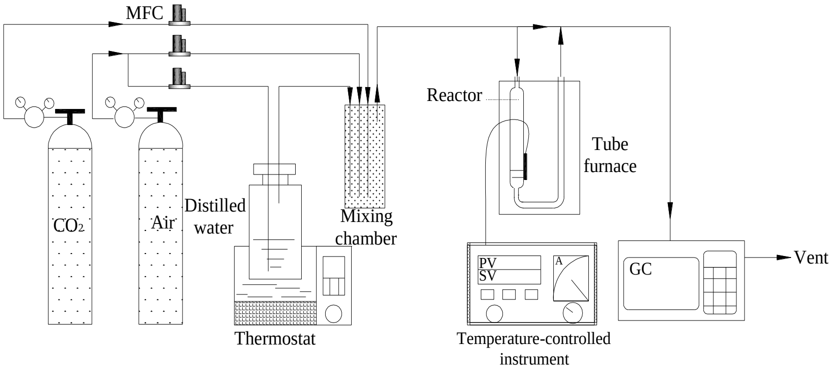

Figure 1. Schematic diagram of the experimental setup for CO_2 adsorption assessment.

3. Results and Discussion

3.1. CO_2 Sorption Performances of Different K_2CO_3-Based Adsorbents

A series of K_2CO_3-based adsorbents were synthesized using the impregnation method, uniformly incorporating a 20% mass percentage of K_2CO_3 onto various support materials. The supports selected included aluminum oxide (Al_2O_3), coconut shell activated carbon (CSAC), coal-based activated carbon (CAC), and a series of molecular sieves, namely, zeolite ZSM-5, zeolite MCM-41, zeolite 5A, zeolite β, and zeolite NaY. The loading amount of K_2CO_3 was determined according to the literature [46,47], and the supports were chosen for their heterogeneous pore texture and abundant porosities. A comparison of the CO_2 adsorption capacities for these adsorbents, each loaded with 20% K_2CO_3, was conducted under identical conditions, as depicted in Figure 2.

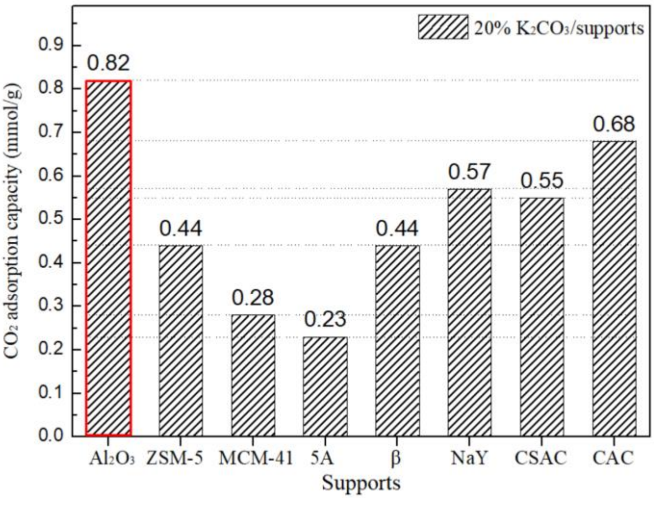

Figure 2. CO_2 adsorption capacities of the 20% K_2CO_3/supports under the conditions: 10 vol% CO_2 in air, 298 K adsorption temperature.

Porous solid materials are primarily characterized by the physical adsorption of CO_2. Given that our study focuses on a low concentration of CO_2 at 10%, the physical adsorption effect results in a low adsorption capacity, which can fall below the detection limit of gas chromatography. Consequently, the CO_2 adsorption capacity of the supports is not depicted here. For the adsorbents with 20% K_2CO_3 loading, the 20% K_2CO_3/Al_2O_3 adsorbent exhibits a higher CO_2 adsorption capacity compared to the other adsorbents. This superior performance may be attributed to the unique pore structure of Al_2O_3, which facilitates a homogeneous distribution of K_2CO_3 and promotes efficient contact between CO_2 and the alkaline adsorption sites.

Due to its excellent performance, the pore structure and morphology of the Al_2O_3 support were further optimized by using different preparation conditions. Two types of Al_2O_3 were synthesized using different precursor solutions, as described in the experimental section. In Scheme 1, Al_2O_3-1 was formed by adding urea and F127 to sodium aluminate as the aluminum source. In Scheme 2, Al_2O_3-2 was produced by incorporating urea into a solution containing aluminum nitrate as the aluminum source. Both Al_2O_3-1 and Al_2O_3-2 were then subjected to impregnation with 20% K_2CO_3, resulting in CO_2 adsorption capacities of 0.69 mmol g^{-1} and 1.12 mmol g^{-1}, respectively.

The 20% K_2CO_3/Al_2O_3-2 adsorbent exhibited a significantly higher CO_2 adsorption capacity than 20% K_2CO_3/Al_2O_3-1. Thus, further adjustments were made to the Al_2O_3-2 support, including varying the hydrothermal reaction time, temperature, and the molar ratio of urea to aluminum nitrate nonahydrate ($Al(NO_3)_3 \cdot 9H_2O$) during the hydrothermal process. The obtained results are presented in Figure 3.

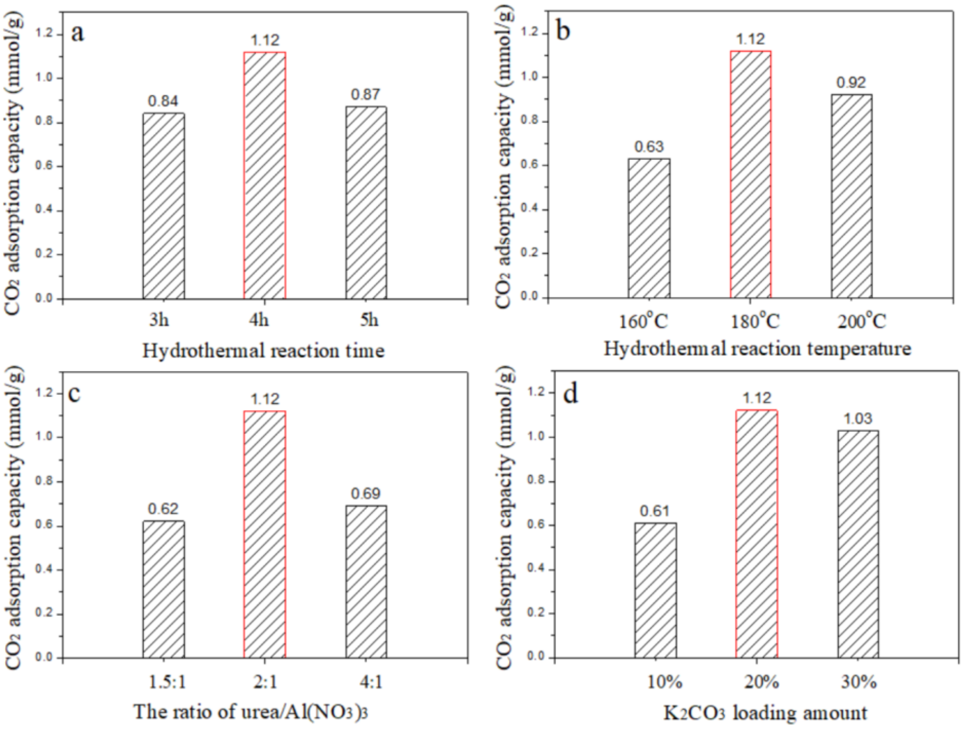

Figure 3. (**a**–**d**) CO_2 adsorption capacities of 20% K_2CO_3/Al_2O_3-2 adsorbents by varying preparation conditions.

Figure 3a,b show the effects of hydrothermal reaction time and temperature on the preparation process, respectively. Clearly, either an excessively short reaction time or an undesirably low temperature can hinder the formation of Al_2O_3 crystals with perfection. Conversely, an excessively long reaction time or high temperature can damage the pore structure, affecting the CO_2 adsorption performance of Al_2O_3 after K_2CO_3 loading. Figure 3c illustrates the optimization of the urea/$Al(NO_3)_3$ ratio. Proper amounts of urea and $Al(NO_3)_3$ are crucial for precise Al_2O_3 formation; excess amounts can lead to impurities, reducing the product's purity and performance. Therefore, the optimal preparation conditions were determined to be a 2:1 molar ratio of urea to $Al(NO_3)_3 \cdot 9H_2O$ in the precursor solution, with a hydrothermal reaction at 180 °C for 4 h.

Figure 3d exhibits the effect of varying the K_2CO_3 loading amount, indicating that the optimal loading is 20%. At a 10% loading, there are insufficient alkaline active sites on the adsorbent surface, resulting in lower CO_2 adsorption capacity. Conversely, at a 30% loading, an excess of K_2CO_3 may block the pores, leading to the uneven dispersion of active sites, which in turn results in a lower utilization rate and a subsequent decrease in CO_2 adsorption capacity.

Based on the optimal adsorption capacity attained, which was 1.12 mmol g^{-1}, the utilization rate of K_2CO_3 was evaluated. Theoretical calculations, derived from the chemical reaction equation $K_2CO_3 + H_2O + CO_2 \rightleftharpoons 2KHCO_3$, suggest that each gram of the adsorbent is capable of potentially adsorbing up to 1.45 mmol g^{-1} of CO_2. As a result, the calculated maximum utilization rate for K_2CO_3 is approximately 77%.

3.2. Characterization of Self-Prepared Al_2O_3

The Al_2O_3 powders, synthesized using two different precursor solutions, have been subjected to comprehensive characterization and analysis. The X-ray diffraction (XRD) patterns for the Al_2O_3-1 and Al_2O_3-2 samples are presented in Figure 4. The patterns show that the reflective peaks observed in both samples are definitively attributed to cubic γ-Al_2O_3 [48], indicating a complete transformation achieved through the calcination process. In addition, the absence of any characteristic peaks from other crystalline impurities suggests that the samples exhibit an exceptionally high degree of purity. Notably, Al_2O_3-2 exhibits narrower diffraction peaks and relatively elevated peak intensities, indicating superior crystallinity and enhanced crystal quality. High crystallinity γ-Al_2O_3 may exhibit fewer defects and structural distortions, which is beneficial for improving the pore structure of the support and achieving a uniform distribution of surface active-sites [49].

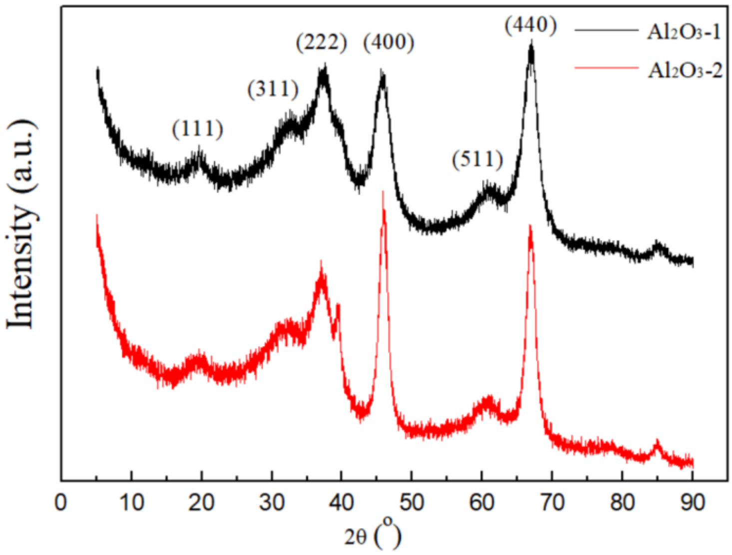

Figure 4. XRD patterns of Al_2O_3-1 and Al_2O_3-2.

The morphologies of Al_2O_3-1 and Al_2O_3-2 were examined using scanning electron microscopy (SEM). The spherical morphologies of Al_2O_3-1 are clearly observable in Figure 5a,b. It has been reported that hydrogen bonds between the surface of aluminum hydroxide (the precursor to γ-Al_2O_3) and the structure-directing agent molecules can reduce the free energy of the crystals, leading to the formation of low-dimensional nanosheets [50]. These nanosheets tend to aggregate to minimize the exposed area and thus reduce surface energy. Consequently, hierarchical porous γ-Al_2O_3 particles with a similarly spherical structure were formed through the directed self-assembly mediated by F127. The hierarchical porous structure not only accommodates K_2CO_3, providing basic active sites for CO_2 adsorption, but also provides diffusion channels for CO_2. Figure 5c depicts a low-magnification SEM image of Al_2O_3-2, showing that the sample is composed of well-dispersed spindle-like aggregates, and the irregular agglomerates are almost negligible, indicating the high quality and purity of the spindle-like aggregates. Figure 5d, a high-magnification SEM image, reveals that the three-dimensional spindle-like particles consist of well-aligned nanoplates with spindle-like edges and rough surfaces.

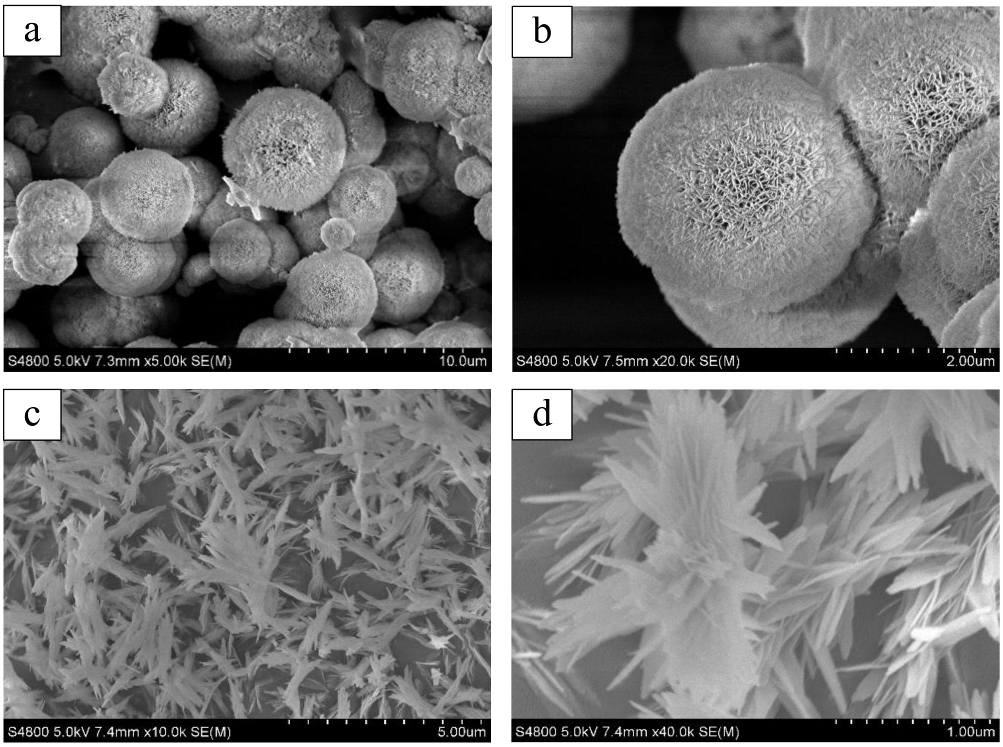

Figure 5. SEM images of Al_2O_3-1 (**a**,**b**) and Al_2O_3-2 (**c**,**d**).

Obviously, compared to the spherical structure of Al_2O_3-1, the three-dimensional spindle-shaped pore structure in Al_2O_3-2 may be more conducive to the impregnation and uniform dispersion of K_2CO_3. It is likely that the spindle-like porous structure not only facilitates the entry of K_2CO_3 but also enables the accommodation and dispersion of more of it. After the loading of K_2CO_3, there is sufficient space for CO_2 diffusion to be captured by active sites. In contrast, the pore size of the spherical structured Al_2O_3-1 appears relatively narrower, and after K_2CO_3 loading, it is prone to blockage, leading to greater resistance to CO_2 diffusion within its interior.

The hierarchical structures of the two as-prepared Al_2O_3 samples were characterized using N_2 adsorption–desorption isotherms, as shown in Figure 6. It is evident that the nitrogen adsorption isotherms for both materials have been classified as type IV according to the International Union of Pure and Applied Chemistry (IUPAC) [51], signifying the basic characteristic of mesoporous materials. The hysteresis loop exhibited by Al_2O_3-2 is typically characterized as type H1, which is a feature commonly observed in mesoporous materials with a relatively uniform pore size distribution. The weakly pronounced condensation steps, indicative of small mesopores, and the narrow hysteresis loop observed at high relative pressures reflect the textural larger pores that are formed between plate-like particles. It is documented in the literature that small mesopores, with diameters less than 4 nm, are formed between primary crystallites, while larger mesopores, with diameters greater than 20 nm, are formed between the secondary aggregated particles [52].

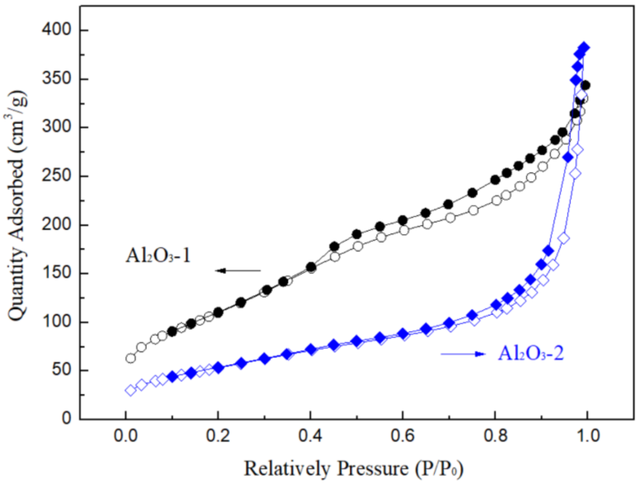

Figure 6. N_2 adsorption (hollow) and desorption (solid) isotherms of Al_2O_3-1 and Al_2O_3-2.

The Al_2O_3-1 curves display a type H3 hysteresis loop, characterized by the absence of a clear saturation adsorption platform. These curves indicate the presence of weak condensation steps, which are associated with the formation of larger slit-like mesopores between plate-like particles [45]. Additionally, a slightly wider hysteresis loop is observed within the relative pressure range of 0.4 to 1.0. The wider hysteresis loop is attributed to the irregularity of the pore structure. Generally, the width of the hysteresis loop is indicative of the connectivity between pores: a wider loop may suggest a lower degree of connectivity, while a narrower loop indicates a higher degree of connectivity between the pores. Obviously, the superior connectivity of the pore structure in Al_2O_3-2 is more favorable for the loading of K_2CO_3 solution. Super connectivity allows for the uniform dispersion of K_2CO_3 within the pore channels, preventing channel blockage and, in turn, facilitating the diffusion of CO_2. The enhanced connectivity also promotes contact with a greater number of active sites, thereby increasing the adsorption capacity for CO_2.

The pore structure parameters of the samples, including specific surface area, pore volume, and average pore size, are listed in Table 1. It can see that Al_2O_3-1 exhibits a higher BET surface area; however, this does not necessarily imply that more active sites would be exposed to CO_2 after K_2CO_3 loading. The relatively small average pore diameter may lead to significant pore blockage, resulting in the loss of a large number of active sites. In contrast, Al_2O_3-2, which has a similar total pore volume to Al_2O_3-1, exhibits a much larger average pore diameter and better pore connectivity, as inferred from Figure 6. Consequently, this facilitates the uniform dispersion of K_2CO_3, the exposure of alkaline active sites, and the reduction of CO_2 diffusion resistance, thereby further enhancing the utilization rate of active sites and the CO_2 adsorption capacity.

Table 1. Textual characteristics of Al_2O_3-1 and Al_2O_3-2.

Preparation Method	**BET Surface Area (m^2 g^{-1})**	**Pore Volume (cm^3 g^{-1})**	**Average Pore Diameter (nm)**
Al_2O_3-1	417	0.53	4.9
Al_2O_3-2	196	0.59	11.89

Figure 7 reveals that Al_2O_3-1 has a higher BET surface area and a smaller average pore diameter due to its abundance of micropores, whereas Al_2O_3-2, with a greater number of mesopores and macropores, has a lower BET surface area and a larger average pore diameter.

In summary, the connectivity of the pores and the large pore diameter of the support are deduced as key factors for achieving high CO_2 adsorption capacity. The comparative schematic of CO_2 diffusion in the interconnected and non-interconnected pore channels is depicted in Figure 8. It is evident that the interconnected pores significantly facilitate the diffusion of CO_2.

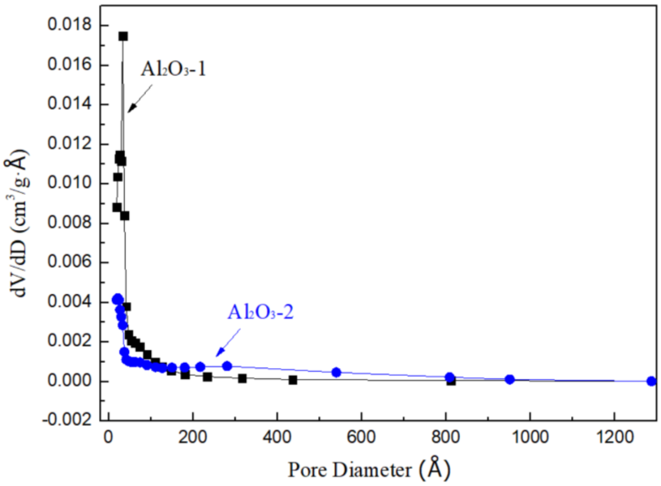

Figure 7. Pore size distributions of Al_2O_3-1 and Al_2O_3-2.

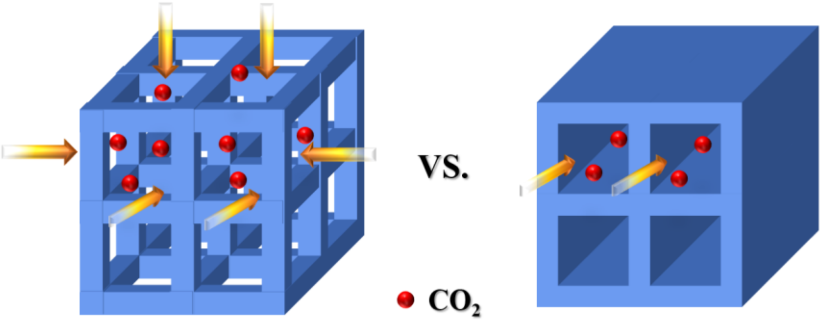

Figure 8. A comparative schematic of CO_2 diffusion in interconnected and non-interconnected pore channels. The arrow represents the direction of molecular diffusion.

The thermal stability of Al_2O_3-1 and Al_2O_3-2 was examined using TGA, as depicted in Figure 9. Neither of the two aluminum oxide samples exhibited weight loss or endothermic peaks throughout the temperature-programmed process, suggesting that the aluminum oxide support is thermally stable at the adsorption and desorption temperatures of 25 °C and 350 °C. Consequently, the K_2CO_3/Al_2O_3 sorbents have the potential to be reused multiple times without losing amine sites.

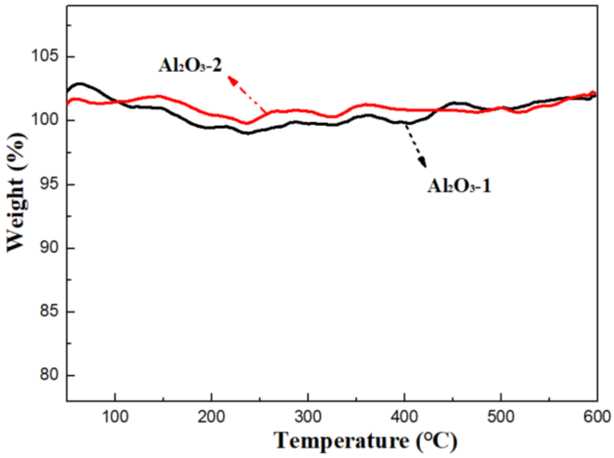

Figure 9. TGA curves of Al_2O_3-1 and Al_2O_3-2.

3.3. Recycling Performance

The regeneration performance of the adsorbent was evaluated and is depicted in Figure 10. Typically, after the CO_2 sorption process in a closed-loop environmental control system, adsorbents are regenerated by increasing the temperature or introducing high-temperature steam. In our experiment, the used adsorbents were regenerated at 350 °C, a temperature at which the reacted products can be completely regenerated [46]. After 10 cycles, the CO_2 adsorption capacity of the 20% K_2CO_3/Al_2O_3 sorbent showed virtually no decline, demonstrating that the prepared sorbent can be reused repeatedly while maintaining its CO_2 adsorption capacity.

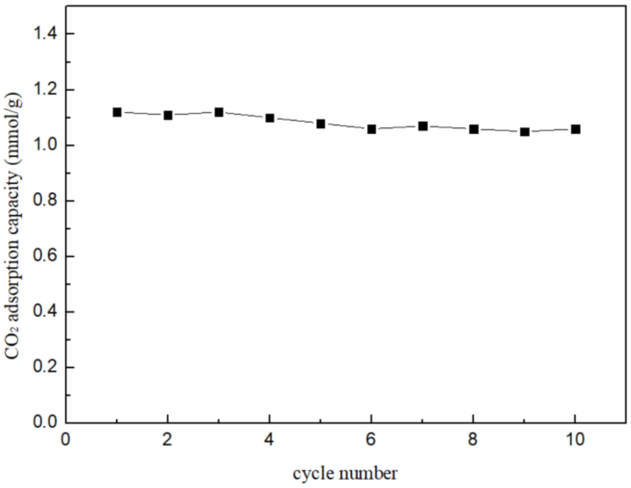

Figure 10. Recycling performance of 20% K_2CO_3/Al_2O_3-2 adsorbent after 10 cycles.

4. Conclusions

A series of K_2CO_3-based adsorbents were synthesized in this work. The CO_2 sorption performance was investigated in detail under ambient temperature conditions and at a CO_2 concentration of 10% using a fixed-bed flow sorption system, equipped with gas flow controllers and an integrated online gas chromatograph system. A 20 wt.% loading of K_2CO_3 was impregnated onto various supports, including Al_2O_3, zeolites ZSM-5, MCM-41, 5A, β, and NaY, CSAC, and CAC. Among these supports, Al_2O_3 was identified as the superior support, leading to further optimization of its pore structure by varying the preparation conditions to enhance CO_2 adsorption capacity. The sorbent of 20% K_2CO_3/Al_2O_3-2 achieved the maximum CO_2 adsorption capacity of 1.12 mmol g^{-1}, and the utilization rate of K_2CO_3 was 77%. The pore volume and pore size distribution were found to significantly influence CO_2 adsorption, as larger, interconnected pores enabled the uniform dispersion of the alkaline active sites, thereby enhancing the utilization of K_2CO_3. Moreover, the optimum adsorbent demonstrated full regenerability at 350 °C, highlighting its excellent recyclability. The K_2CO_3/Al_2O_3 sorbent may be an excellent choice for CO_2 removal in coal-fired power plants.

Author Contributions: Investigation, Conceptualization, Formal analysis, Writing—original draft, and Funding acquisition, Y.Z.; Writing—review and editing, and Supervision, J.H.; Investigation and Formal analysis, X.W.; Investigation, S.M. All authors have read and agreed to the published version of the manuscript.

Funding: This research was funded by the Scientific Research Project of Tianjin Education Commission (No. 2023KJ255).

Data Availability Statement: Data are available on request due to restrictions.

Conflicts of Interest: The authors declare no conflicts of interest.

References

1. Alalaiwat, D.; Khan, E. Post-combustion carbon capture process modeling, simulation, and assessment of synergistic effect of solvents. *Int. J. Greenh. Gas Control* **2024**, *135*, 104145. [CrossRef]
2. Sandip, K.D.; Dong, W.; Ha, J.K.D. Integrated CO_2 capture and electrochemical upgradation: The underpinning mechanism and techno-chemical analysis. *Chem. Soc. Rev.* **2023**, *52*, 5744–5802.
3. Subramanian, N.; Madejski, P. Analysis of CO_2 capture process from flue-gases in combined cycle gas turbine power plant using post-combustion capture technology. *Energy* **2023**, *282*, 128311. [CrossRef]
4. Zhang, G.; Ma, L.; Pourkashanian, M. A porous medium approach to the 3D modelling of an entire rotating packed bed for post-combustion carbon capture. *Chem. Eng. Sci.* **2023**, *274*, 118687. [CrossRef]
5. Sridhar, P.; Kumar, A.; Karimi, F.I.A. Technoeconomic evaluation of post-combustion carbon capture technologies on-board a medium range tanker. *Comput. Chem. Eng.* **2024**, *181*, 108545. [CrossRef]
6. Rashidi, H.; Emailprotected, E. Performance of Water-Lean Solvent for Post combustion Carbon Dioxide Capture in a Process-Intensified Absorber: Experimental, Modeling, and Optimization Using RSM and ML. *Ind. Eng. Chem. Res.* **2023**, *62*, 20821–20832.
7. Komati, S.; Suresh, A.K. CO_2 absorption into amine solutions: A novel strategy for intensification based on the addition of ferrofluids. *J. Chem. Technol. Biotechnol.* **2010**, *83*, 1094–1100. [CrossRef]
8. Aha, A.K.; Biswas, A.K.; Bandyopadhyay, S.S. Absorption of CO_2 in a sterically hindered amine: Modeling absorption in a mechanically agitated contactor. *Sep. Purif. Technol.* **1999**, *15*, 101–112.
9. Baran, P.; Zarbska, K.; Czuma, N. CO_2 adsorption properties of char produced from brown coal impregnated with alcohol amine solutions. *Environ. Monit. Assess.* **2016**, *188*, 416. [CrossRef]
10. Papatryfon, X.L.; Molchan, I.S.; Heliopoulos, N.S. CO_2 Capture Efficiency, Corrosion Properties, and Ecotoxicity Evaluation of Amine Solutions Involving Newly Synthesized Ionic Liquids. *Ind. Eng. Chem. Res.* **2014**, *53*, 12083–12102. [CrossRef]
11. Sekizkardes, A.K.; Wang, P.; Hoffman, J. Amine-functionalized porous organic polymers for carbon dioxide capture. *Materials Advances* **2022**, *3*, 6668–6686. [CrossRef]
12. Gray, M.L.; Champagne, K.J.; Fauth, D. Performance of immobilized tertiary amine solid sorbents for the capture of carbon dioxide. *Int. J. Greenh. Gas Control* **2008**, *2*, 3–8. [CrossRef]
13. Schladt, M.J.; Filburn, T.P.; Helble, J.J. Supported amine sorbents under temperature swing absorption for CO_2 and moisture capture. *Ind. Eng. Chem. Res.* **2007**, *46*, 1590–1597. [CrossRef]
14. Dillon, E.P.; Crouse, C.A.; Barron, A.R. Synthesis, characterization, and carbon dioxide adsorption of covalently attached polyethyleneimine-functionalized single-wall carbon nanotubes. *ACS Nano* **2008**, *2*, 156–164. [CrossRef]
15. Ye, Q.; Jiang, J.; Wang, C.; Liu, Y.; Pan, H.; Shi, Y. Adsorption of low-concentration carbon dioxide on amine-modified carbon nanotubes at ambient temperature. *Energy Fuels* **2012**, *26*, 2497–2504. [CrossRef]
16. Plaza, M.G.; Pevida, C.; Arenillas, A.; Rubiera, F.; Pis, J.J. CO_2 capture by adsorption with nitrogen enriched carbons. *Fuel* **2007**, *86*, 2204–2212. [CrossRef]
17. Aroua, M.K.; Daud, W.M.A.W.; Yin, C.Y.; Adinata, D. Adsorption capacities of carbon dioxide, oxygen, nitrogen and methane on carbon molecular basket derived from polyethyleneimine impregnation on microporous palm shell activated carbon. *Sep. Purif. Technol.* **2008**, *62*, 609–613. [CrossRef]
18. Wang, J.; Chen, H.; Zhou, H.; Liu, X.; Qiao, W.; Long, D.; Ling, L. Carbon dioxide capture using polyethylenimine-loaded mesoporous carbons. *J. Environ. Sci.* **2013**, *25*, 124–132. [CrossRef] [PubMed]
19. Zhao, P.; Yin, Y.; Xu, X.; Yang, D.; Wang, J.; Yang, F.; Zhang, G. Facile fabrication of mesoporosity silica as support for solid amine CO_2 adsorbents with enhanced adsorption capacity and kinetics. *Energy* **2022**, *253*, 124162. [CrossRef]
20. Wang, Y.; Anyanwu, J.T.; Hu, Z.; Yang, R.T. Significantly enhancing CO_2 adsorption on Amine-Grafted SBA-15 by boron doping and acid treatment for direct air capture. *Sep. Purif. Technol.* **2023**, *309*, 123030. [CrossRef]
21. Stuckert, A.N.; Yang, R.T. CO_2 capture from the atmosphere and simultaneous concentration using zeolites and amine-grafted SBA-15. *Environ. Sci. Technol.* **2011**, *45*, 10257–10264. [CrossRef] [PubMed]
22. Wang, R.; Guo, T.; Xiang, X.; Yin, Y.; Guo, Q.; Wang, Y. Antioxidative degradation mechanism of 2-mercaptobenzimidazole modified TEPA-MCM-41 adsorbents for carbon capture from flue gas. *Can. J. Chem. Eng.* **2023**, *101*, 6284–6295. [CrossRef]
23. Ajumobi, O.; Wang, B.; Farinmade, A.; He, J.; Valla, J.A.; John, V.T. Design of Nanostraws in Amine-Functionalized MCM-41 for Improved Adsorption Capacity in Carbon Capture. *Energy Fuels* **2023**, *37*, 12079–12088. [CrossRef]
24. Son, W.J.; Choi, J.S.; Ahn, W.S. Adsorptive removal of carbon dioxide using polyethyleneimine-loaded mesoporous silica materials. *Micropor. Mesopor. Mat.* **2008**, *113*, 31–40. [CrossRef]
25. Zhao, Y.; Zhu, Y.; Zhu, T.; Lin, G. Enhanced CO_2 adsorption over silica-supported tetraethylenepentamine sorbents doped with alkanolamines or alcohols. *Ind. Eng. Chem. Res.* **2018**, *58*, 156–164. [CrossRef]
26. Zhao, C.; Chen, X.; Anthony, E.J.; Jiang, X.; Duan, L.; Wu, Y.; Dong, W.; Zhao, C. Capturing CO_2 in flue gas from fossil fuel-fired power plants using dry regenerable alkali metal-based sorbent. *Prog. Energy Combust.* **2013**, *39*, 515–534. [CrossRef]
27. Yan, M.; Zhang, Y.; Huan, Q.; Song, Y.; Zhou, X.; Wibowo, H.; Yu, C. Effect of operating parameters for CO_2 capture from syngas of supercritical water gasification using $K_2CO_3/\gamma\text{-}Al_2O_3$ composite adsorbent. *Biomass Conv. Bioref.* **2024**, *14*, 3667–3677. [CrossRef]
28. Zhao, C.; Guo, Y.; Li, C.; Lu, S. Carbonation behavior of K_2CO_3/AC in low reaction temperature and CO_2 concentration. *Chem. Eng. J.* **2014**, *254*, 524–530. [CrossRef]

29. Yang, Y.; Zhao, C.; Zeng, P. Hydrophobie interface-assisted synthesis of K_2CO_3/Al_2O_3 adsorbent pellets for CO_2 capture. *Sep. Purif. Technol.* **2023**, *317*, 123933. [CrossRef]
30. Lee, S.C.; Choi, B.Y.; Lee, T.J.; Ryu, C.K.; Ahn, Y.S.; Kim, J.C. CO_2 absorption and regeneration of alkali metal-based solid sorbents. *Catal. Today* **2006**, *111*, 385–390. [CrossRef]
31. Zhao, Z.; Zhang, Y.; Othman, R.M.; Ha, W.; Wang, J.; Wang, T.; Zhong, L.; Wang, J.; Pan, W. CO_2 adsorption by coal fly ash zeolite and modified zeolite-templated carbon. *Process. Saf. Environ.* **2024**, *186*, 151–165. [CrossRef]
32. Kumar, V.; Jadhav, P.; Lokhande, S.K.; Biniwale, R.B.; Labhsetwar, N.K.; Rayalu, S.S. Amine loaded zeolites for carbon dioxide capture: Amine loading and adsorption studies. *Microporous Mesoporous Mater.* **2009**, *121*, 84–89.
33. Xu, X.; Zhao, X.; Sun, L.; Liu, X. Adsorption separation of carbon dioxide, methane and nitrogen on monoethanol amine modified β-zeolite. *J. Nat. Gas Chem.* **2009**, *18*, 167–172. [CrossRef]
34. Huang, Y.; He, X.; Wei, X.; Yue, J.; Jiang, J.; Zhao, C. Experimental and kinetics investigations of low-concentration CO_2 adsorption on several amine-functionalized adsorbents. *Process. Saf. Environ.* **2022**, *160*, 573–583.
35. Quan, C.; Jia, X.; Zhang, K.; Zhang, Y.; Naqvi, S.R.; Amin, N.A.S.; Gao, N. Amine-impregnated silica zeolite from microalgae ash at different calcination temperatures for CO_2 capture. *Int. J. Energ. Res.* **2022**, *46*, 1220–1233. [CrossRef]
36. Siriwardane, R.; Shen, M.; Losch, J. Adsorption of CO_2 on zeolites at moderate temperatures. *Energy Fuels* **2005**, *19*, 1153–1159. [CrossRef]
37. Zhang, J.; Singh, R.; Webley, P.A. Alkali and alkaline-earth cation exchanged chabazite zeolites for adsorption based CO_2 capture. *Microporous Mesoporous Mater.* **2008**, *111*, 478–487. [CrossRef]
38. Lu, C.; Bai, H.; Wu, B.; Su, F.; Hwang, J.F. Comparative study of CO_2 capture by carbon nanotubes, activated carbons, and zeolites. *Energy Fuels* **2008**, *22*, 3050–3056. [CrossRef]
39. Lee, S.C.; Kwon, Y.M.; Ryu, C.Y.; Chae, H.J.; Ragupathy, D.; Jung, S.Y.; Lee, J.B.; Ryu, C.K.; Kim, J.C. Development of new alumina-modified sorbents for CO_2 sorption and regeneration at temperatures below 200 °C. *Fuel* **2011**, *90*, 1465–1470. [CrossRef]
40. Zhao, C.; Chen, X.; Zhao, C. CO_2 absorption using dry potassium-based sorbents with different supports. *Energy Fuels* **2009**, *23*, 4683–4687. [CrossRef]
41. Zhao, C.; Chen, X.; Zhao, C. Multiple-cycles behavior of K_2CO_3/Al_2O_3 for CO_2 capture in a fluidized-bed reactor. *Energy Fuels* **2010**, *24*, 1009–1012. [CrossRef]
42. Zhao, C.; Chen, X.; Zhao, C. Carbonation and active-component-distribution behaviors of several potassium-based sorbents. *Ind. Eng. Chem. Res.* **2011**, *50*, 4464–4470. [CrossRef]
43. Zhao, C.; Chen, X.; Zhao, C.; Wu, Y. K_2CO_3/Al_2O_3 for capturing CO_2 in flue gas from power plants. Part 3: CO_2 capture behaviors of K_2CO_3/Al_2O_3 in a bubbling fluidized-bed reactor. *Energy Fuels* **2012**, *26*, 3062–3068. [CrossRef]
44. Ge, J.; Deng, K.; Cai, W.; Yu, J.; Liu, X.; Zhou, J. Effect of structure-directing agents on facile hydrothermal preparation of hierarchical γ-Al_2O_3 and their adsorption performance toward Cr (VI) and CO_2. *J. Colloid. Interf. Sci.* **2013**, *401*, 34–39. [CrossRef]
45. Cai, W.; Yu, J.; Jaroniec, M. Template-free synthesis of hierarchical spindle-like γ-Al_2O_3 materials and their adsorption affinity towards organic and inorganic pollutants in water. *J. Mater. Chem.* **2010**, *20*, 4587–4594. [CrossRef]
46. Zhao, C.; Guo, Y.; Li, C.; Lu, S. Removal of low concentration CO_2 at ambient temperature using several potassium-based sorbents. *Appl. Energy* **2014**, *124*, 241–247. [CrossRef]
47. Guo, Y.; Zhao, C.; Li, C.; Wu, Y. CO_2 sorption and reaction kinetic performance of K_2CO_3/AC in low temperature and CO_2 concentration. *Chem. Eng. J.* **2015**, *260*, 596–604. [CrossRef]
48. Ma, C.; Chang, Y.; Ye, W.; Shang, W.; Wang, C. Supercritical preparation of hexagonal γ-alumina nanosheets and its electrocatalytic properties. *J. Colloid. Interf. Sci.* **2008**, *317*, 148–154. [CrossRef]
49. Kovarik, L.; Bowden, M.; Khivantsev, K.; Kwak, J.H.; Szanyi, J. Structural complexity of γ-Al_2O_3: The nature of vacancy ordering and the structure of complex antiphase boundaries. *Acta Mater.* **2024**, *266*, 119639. [CrossRef]
50. Zhang, Y.X.; Jia, Y.; Jin, Z.; Yu, X.Y.; Xu, W.H.; Luo, T.; Zhu, B.J.; Liu, J.H.; Huang, X.J. Self-assembled, monodispersed, flower-like γ-AlOOH hierarchical superstructures for efficient and fast removal of heavy metal ions from water. *Cryst. Eng. Comm.* **2012**, *14*, 3005–3007. [CrossRef]
51. Sing, K.S.W. Reporting physisorption data for gas/solid systems with special reference to the determination of surface area and porosity (Recommendations 1984). *Pure. Appl. Chem.* **1985**, *57*, 603–619. [CrossRef]
52. Leofanti, G.; Padovan, M.; Tozzola, G.; Venturelli, B. Surface area and pore texture of catalysts. *Catal. Today* **1998**, *41*, 207–219. [CrossRef]